Supplementary Materials

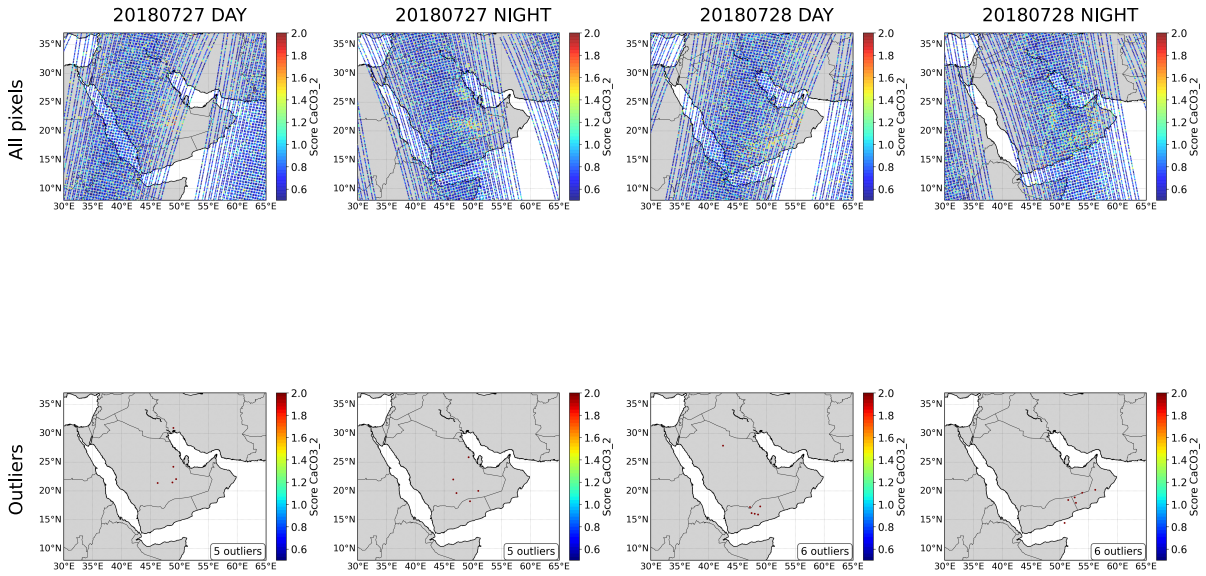


Figure S1. CaCO3_2 scores values between 27th July 2018 and 28th July 2018 (day and night times separated) for all IASI-B pixels processed with IASI-PCA (top panels) and for the detected outliers (bottom panels).

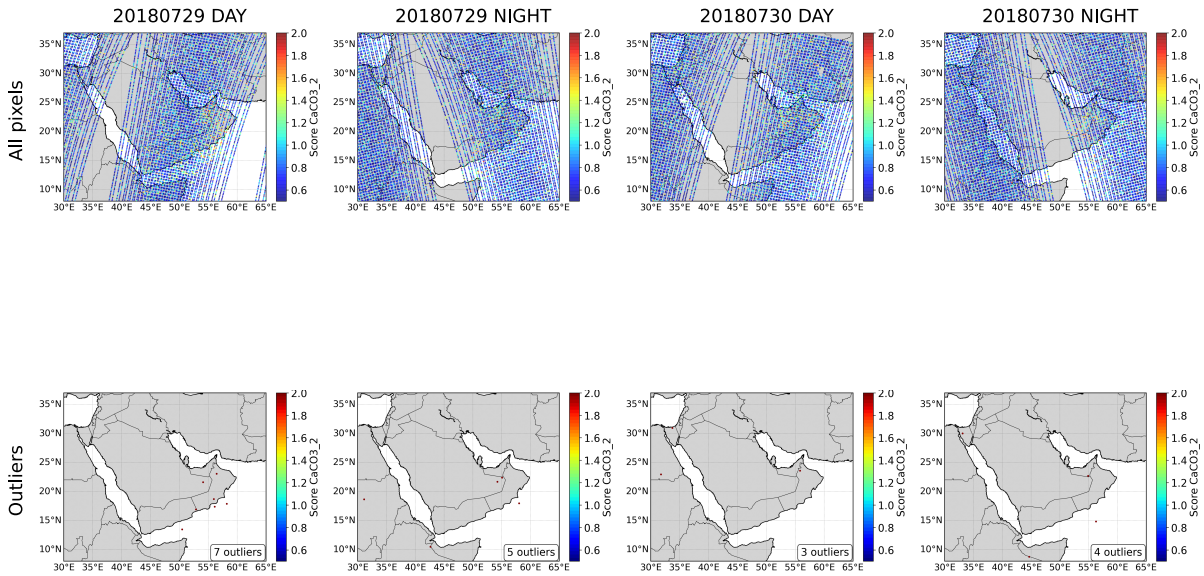


Figure S2. CaCO3_2 scores values between 29th July 2018 and 30th July 2018 (day and night times separated) for all IASI-B pixels processed with IASI-PCA (top panels) and for the detected outliers (bottom panels).

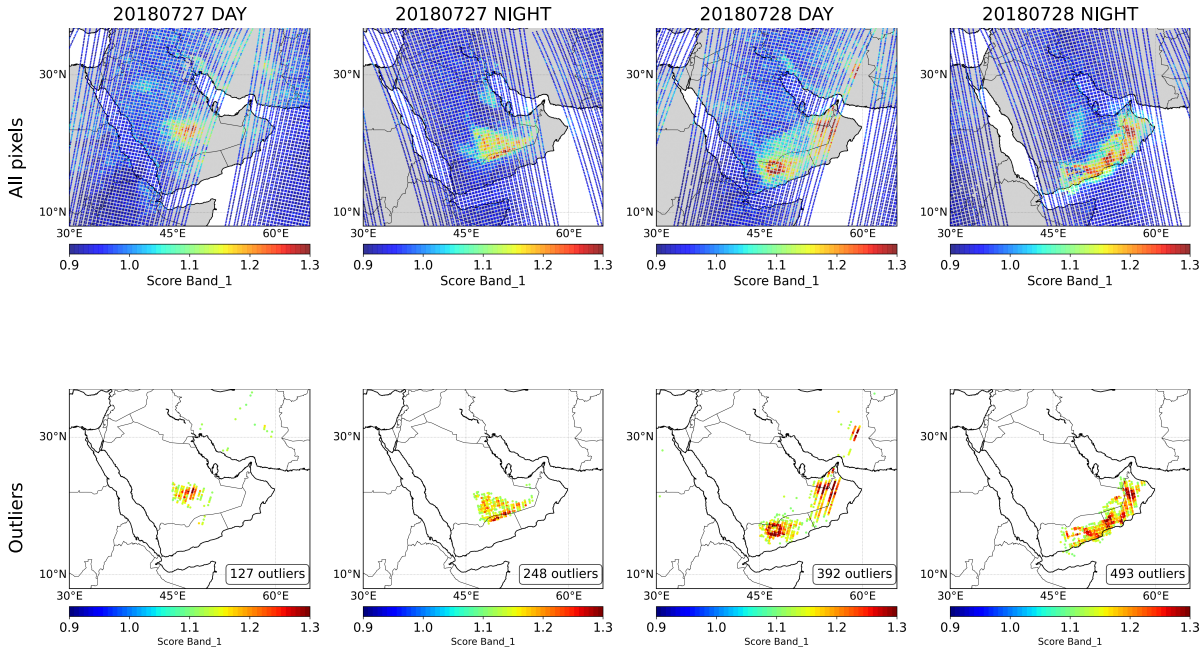


Figure S3. Band_1 scores values between 27th July 2018 and 28th July 2018 (day and night times separated) for all IASI-B pixels processed with IASI-PCA (top panels) and for the detected outliers (bottom panels).

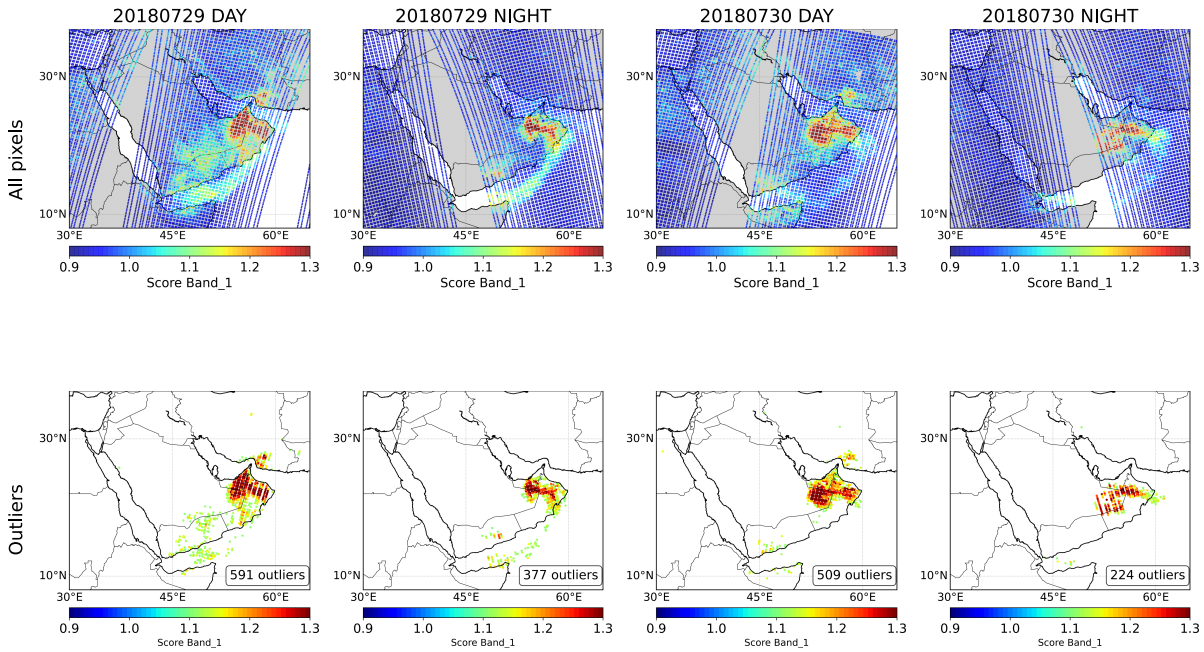


Figure S4. Band_1 scores values between 29th July 2018 and 30th July 2018 (day and night times separated) for all IASI-B pixels processed with IASI-PCA (top panels) and for the detected outliers (bottom panels).

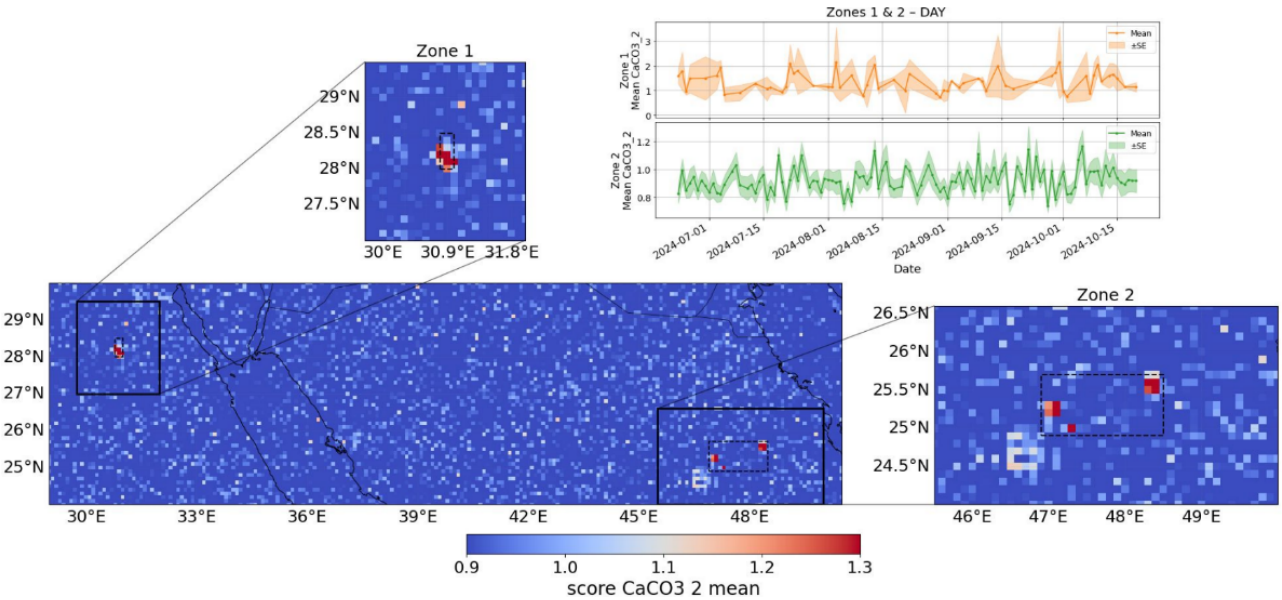


Figure S5. Maps show the mean CaCO3_2 score averaged, in time over the 115 daytime dates and spatially on a 0.1° x 0.1° latitude-longitude grid over Egypt and Saudi-Arabia, with zooms (solid black lines) on zone 1 and zone 2 (black dashed lines). The top right panel shows the time series of the mean CaCO3_2 score for zone 1 (top panel, orange curve) and zone 2 (bottom panel, green curve) over the period studied. Shaded areas for both curves represent the standard error of the mean (noted SE). All available IASI-C IFOVs are considered.

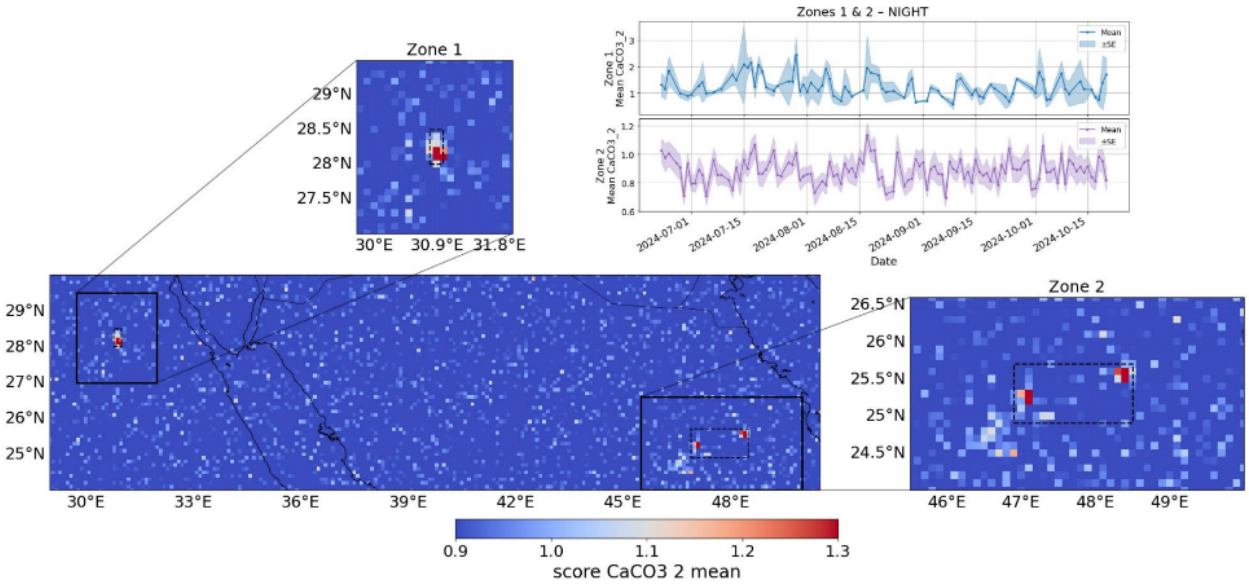


Figure S6. Maps show the mean CaCO3_2 score averaged, in time over the 115 nighttime dates and spatially on a 0.1° x 0.1° latitude-longitude grid over Egypt and Saudi-Arabia, with zooms (solid black lines) on zone 1 and zone 2 (black dashed lines). The top right panel shows the time series of the mean CaCO3_2 score for zone 1 (top panel, blue curve) and zone 2 (bottom panel, purple curve) over the period studied. Shaded areas for both curves represent the standard error of the mean (noted SE). All available IASI-C IFOVs are considered.

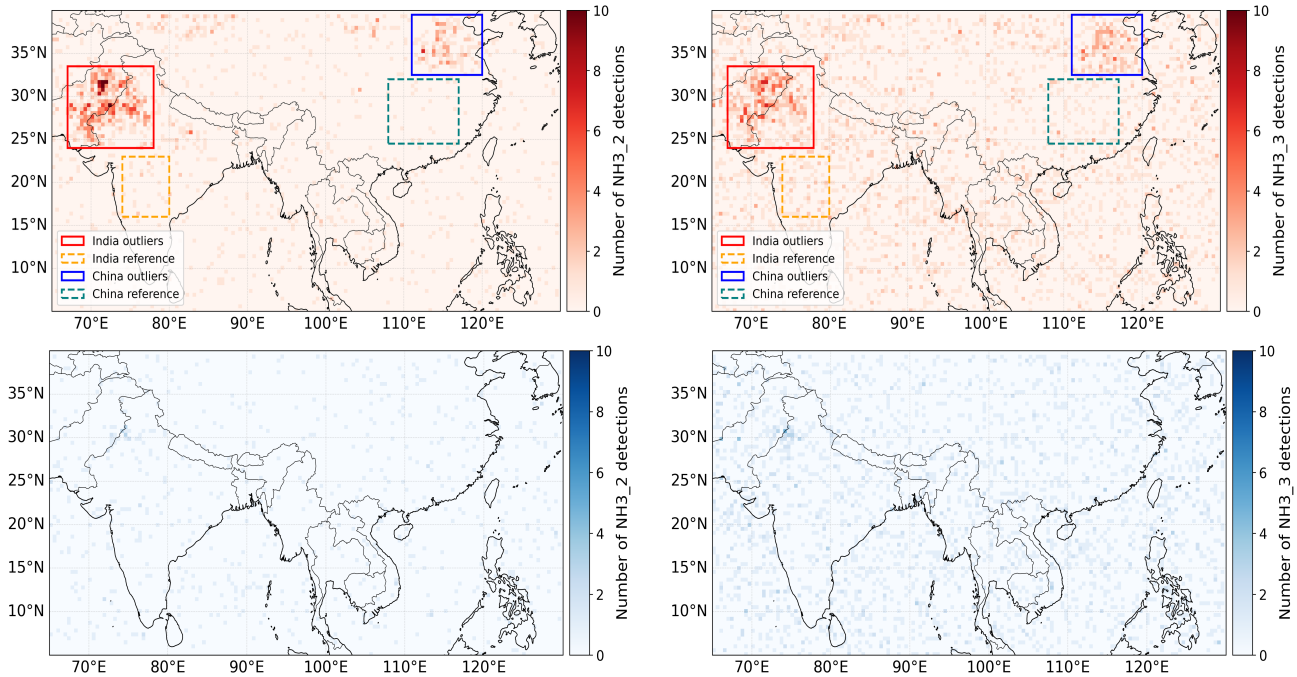


Figure S7. One-year cumulative number of IASI-C detections for the indicators NH3_2 (left panel) and NH3_3 (right panel) computed on a 0.45° x 0.45° latitude-longitude grid. Top and bottom panels show daytime and nighttime results respectively. In the top panels, regions delimited by red and blue solid lines correspond to areas with the largest number of outliers during the day (named "India outliers" and "China outliers"). Orange and teal dashed lines indicate

the associated to "reference" regions, selected for their relatively low number of outliers considered as reference for the unperturbed background (named "India reference" and "China reference").

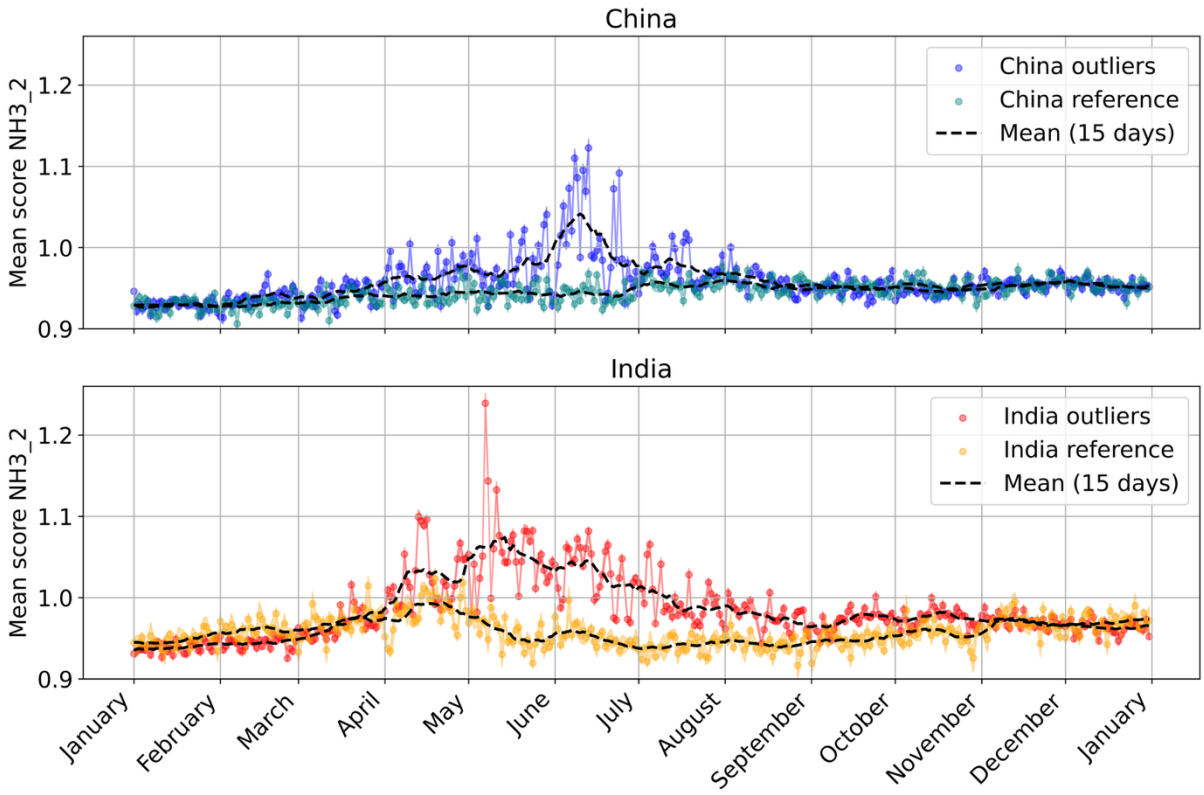


Figure S8. Mean NH3_2 score computed for all available Metop-C IFOVs over the four regions identified during year 2025 (outliers and references zones in China and India, see Fig. S7). The black dashed curves show the 15-days moving average.

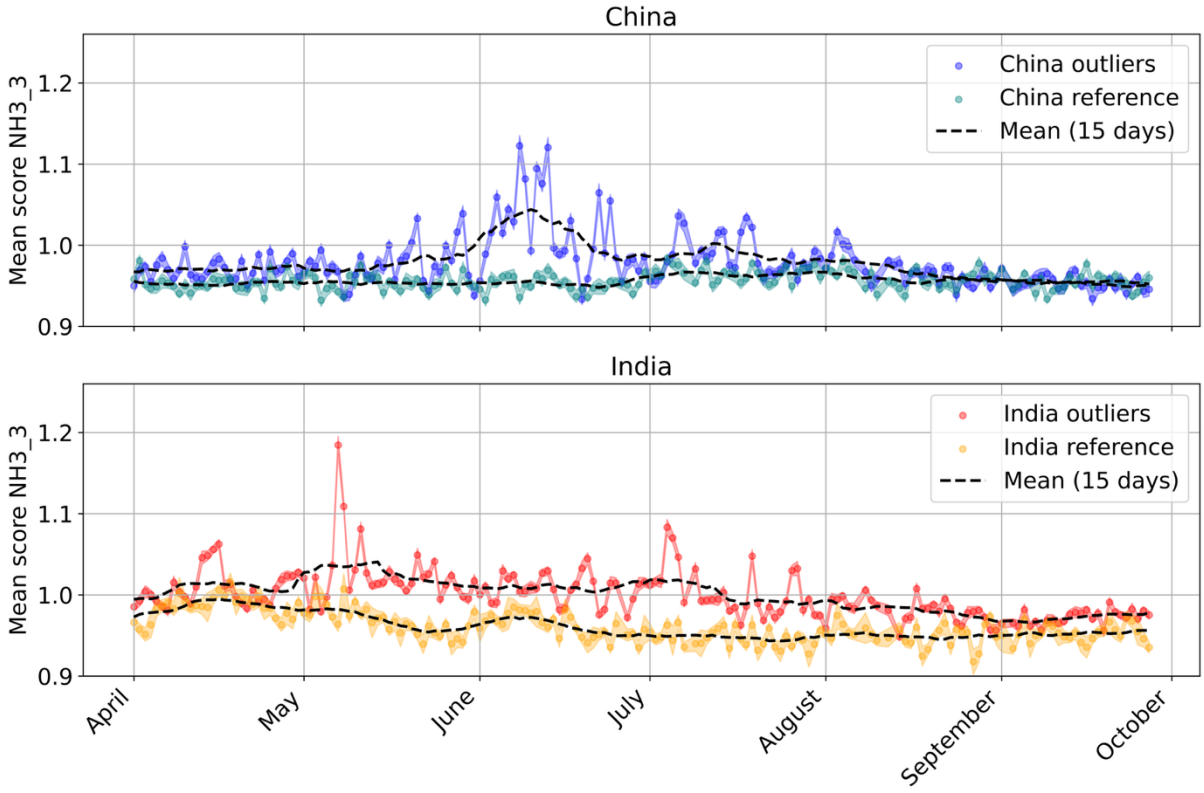


Figure S9. Mean NH3_3 score computed for all available Metop-C IFOVs over the four regions identified during year 2025 (outliers and references zones in China and India, see Figure S7). The black dashed curves show the 15-days moving average.

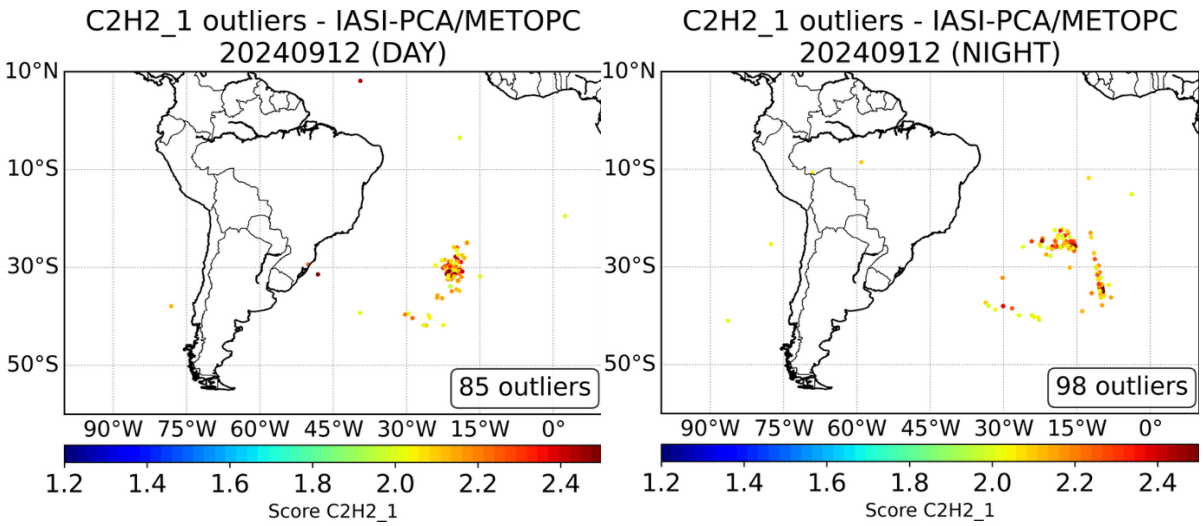


Figure S10. IASI-C outlier scores maps for C2H2_1 over South America and the South Atlantic Ocean. Left: daytime of September 12, 2024. Right: nighttime of September 12, 2024. This date corresponds to the detection peaks of C2H2_1.

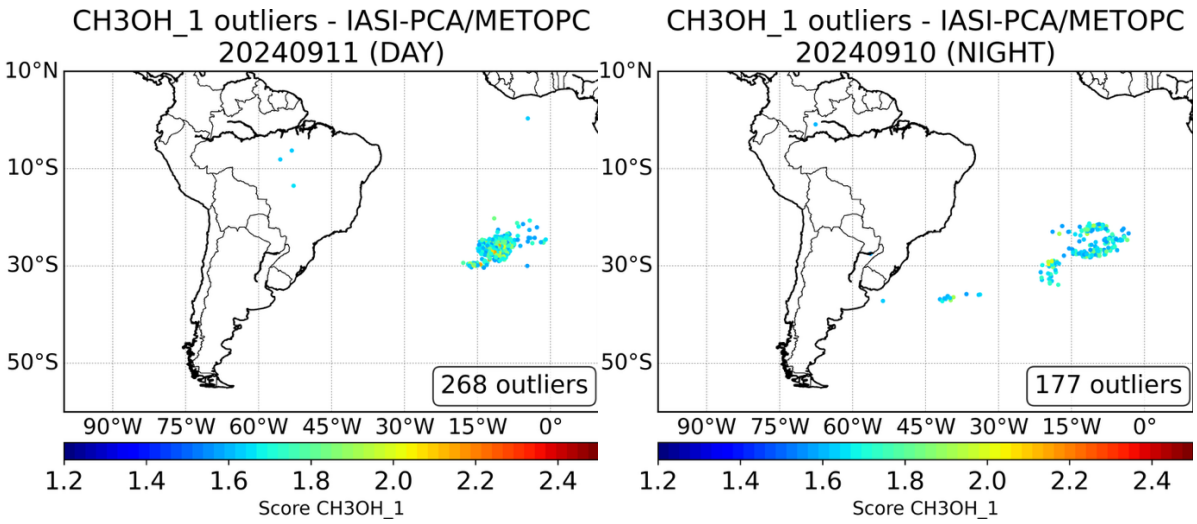


Figure S11. IASI-C outlier scores maps for CH3OH_1 over South America and the South Atlantic Ocean. Left: daytime of September 11, 2024. Right: nighttime of September 10, 2024. These dates correspond to the detection peaks of CH3OH_1.

Dataset S1. Subset of IASI-PCA processing results for the case studies presented in this study, provided to reproduce selected results.
The details can be found at: https://github.com/spascia/sm-iasi-pca-paper-pipien-et-al-2026/releases/tag/published (accessed on 26 July 2026).